ADVANCES IN MATERIALS SCIENCE, Vol. 25, No. 3(85), September 2025

DOI: 10.2478/adms-2025-0013

Kamel Chadi [1,2], Nourredine Belghar[2,3,4], Mohammed Lachi [5], Fuad Khoshnaw[6]*

[1] *Research Centre in Industrial Technologies (CRTI), Cheraga, 16014, Algeria*
[2] *Eco-Materials, Chemical Processes and Sustainable Development Laboratory, Biskra, Algeria*
[3] *Abbas LaghrourUniversity of Khenchela, Algeria*
[4] *Lab. of Materials and Energy Engineering, LGEM, University of Mohamed KhiderBiskra, Algeria*
[5] *ITheMM - Institut de Thermique, Mécanique, Matériaux. Université de Reims Champagne-Ardenne, France*
[6] *School of Engineering and Sustainable Development, De Montfort University, Leicester, U.K.*

* *fuad.khoshnaw@dmu.ac.uk*

NUMERICAL INVESTIGATION OF THERMAL PERFORMANCE IN LIQUID COOLING SERPENTINE MINI-CHANNEL HEAT SINK WITH VARIOUS INLET/OUTLET POSITIONS

ABSTRACT

This study aims to investigate and optimize the thermal dissipation of a constant heat flux source by conducting a numerical analysis of four serpentine mini-channel heat sink configurations, each characterized by different inlet and outlet arrangements for the cooling fluid. The cooling system under study consists of an upper part made of ABS copolymer resin, incorporating the fluid inlets and outlets (water), and a lower part made of aluminum, which contains the serpentine mini-channel heat sink. The analyzed configurations included four cases: First: a single inlet and a single outlet, Second: two inlets and one outlet, Third: one inlet and two outlets, and Fourth: a variation of the third model with reversed inlet and outlet positions. Numerical simulations, performed using the finite volume method, cover a Reynolds number range from 200 to 600. The analysis focuses on flow behavior, temperature distributions, pressure drop, thermal resistance, the average Nusselt number and the performance evaluation factor (PEF). The results indicate that the configurations with two inlets and one outlet (Case 2) and the reversed inlet/outlet configuration (Case 4) significantly enhance cooling compared to the other configurations. However, the two-inlet, one-outlet case also results in a higher pressure drop. At a Reynolds number of 600, Case 2 achieves the best thermal performance with an average Nusselt number of 20.79 and a minimum thermal resistance of 0.228K/W, while Case 3 exhibits the lowest efficiency. These findings help identify optimal configurations for cooling high heat flux electronic components.

Keywords: *Serpentine mini-channel, liquid cooling, heat sink, thermal performance, numerical simulation*

INTRODUCTION

A serpentine mini-channel heat sink is a compact and highly efficient thermal management solution, particularly suited for systems that require significant heat dissipation in limited spaces. It features a network of small, serpentine-shaped channels through which a coolant flows. This design maximizes the heat transfer surface area and induces turbulent flow, both of which enhance cooling performance. These heat sinks are widely used in

Received: 10.05.2025; Received in revised form: 13.07.2025; Accepted: 03.09.2025

applications such as electronic device cooling, high-performance computing systems, and thermal regulation of critical components, ensuring operational stability and reliability. Both experimental and computational studies have consistently shown their capability to achieve high heat transfer rates, making them a key choice for advanced thermal solutions. Researchers [1] have continuously sought to improve the performance of serpentine mini-channel heat sinks by exploring various design and operational parameters. These efforts span multiple directions, including optimizing channel geometry (such as channel size, curvature, and aspect ratio), enhancing coolant flow characteristics through adjustments in flow rate and Reynolds number, and experimenting with different coolant types, including nanofluids with superior thermal properties. Additionally, studies have focused on selecting high thermal conductivity materials for the heat sink structure, refining inlet and outlet configurations to achieve uniform flow distribution, and applying surface enhancements like micro-structures or vortex generators to promote turbulence. Each of these strategies aims to increase heat transfer efficiency while minimizing pressure drop, contributing to more compact and reliable thermal management systems. Tariq et al. [2] evaluated the thermal performance of an MCHS by studying the effect of plate thickness on heat transfer. Their results, compared with data from the literature on heat sinks without plates, revealed a significant temperature reduction for a plate thickness of 0.2 mm, with decreases of 12.5% and 16.2% for fin spacings of 0.5 mm and 1.0 mm, respectively. Ghadhban and Jaffal [3] numerically and experimentally studied the flow and heat transfer behavior in multiple micro-channel heat sinks (MM-CHS). By testing four channel structures (straight, wavy, interrupted wavy, and ribbed wavy), they demonstrated that ribbed wavy channels provide superior heat dissipation and reduce wall temperatures.

Chadi et al. [4] and Mahmoud et al. [5] explored the influence of micro and mini-channel geometry and configurations on thermal performance. Their studies highlighted that the integration of fins and lateral grooves effectively enhances heat dissipation, with significant improvements in Nusselt number and energy efficiency.

Many researchers have focused on the flow characteristics of coolant to improve heat transfer rates. Gorzin et al. [6] conducted an experimental analysis of flow and heat transfer characteristics in a ribbed labyrinth serpentine mini-channel heat sink, varying the rib spacing (12, 15, and 18 cm). Pure water was used as the cooling fluid, with a flow rate ranging from 0.0017 to 0.008 kg/s. The study compared three heat sinks with different rib spacings against a ribless labyrinth heat sink and a straight heat sink. The results revealed that, at a flow rate of 0.0017 kg/s, the base temperature of the ribbed heat sink was 7.9% and 13.9% lower than that of the ribless labyrinth heat sink and the straight heat sink, respectively. Mustafa and Ghani [7] conducted an analytical study of flow and heat transfer characteristics in an MCHS, testing four fin shapes (teardrop, pyramidal, conical, and oval) for Reynolds numbers ranging from 100 to 1000. They found that the conical configuration provided the best thermal performance, with a maximum efficiency factor of 2.25 at Re = 1000.

Some studies focused on the use of nanofluids to improve heat sink performance. Afshari and Muratcobanoglu [8] conducted a numerical study on a block-based heat exchanger designed for electronic processor cooling. They assessed the thermal performance of a Fe_3O_4/water nanofluid at a volumetric concentration of 0.2%, comparing two block configurations (spiral and serpentine) with a configuration using water as the cooling fluid. The analysis of the nanofluid's thermophysical properties was performed using theoretical equations and experimental data. Ataei et al. [9] carried out an experimental study on heat transfer in an aluminum MCHS with rectangular sections, using different nanofluids (TiO_2-water, Al_2O_3-water, and an Al_2O_3/TiO_2-water mixture) at a concentration of 0.5%. The study examined the impact of the Reynolds number, ranging from 400 to 1000, on the thermal performance of the heat sink. The results showed a significant improvement in heat transfer with nanofluids compared to water, with an increase in the heat transfer coefficient of up to 16.91%. Saleem and Heidarshenas [10] conducted a numerical simulation to investigate the thermal performance of a wavy wall microchannel heat sink (WWMCHS) using ANSYS FLUENT, based on the SIMPLE algorithm and the finite volume method. In this study, water was used as the base fluid, along with nanofluids composed of alumina/water and copper oxide/water at concentrations ranging from 0% to 2%. The authors reported that the addition of 2% nanoparticles of aluminum oxide and copper oxide to the base fluid (water), at a Reynolds number of 500, reduced the maximum temperature to 2.55 °C and to 2.38°C, respectively.

Moreover, some researchers have optimised the inlet and outlet configurations to achieve better thermal performance of the heat sink. Mahmood et al. [11] investigated the influence of fluid inlet position, reverse and parallel flow configurations, in addition to the efficiency of mini-channel heat sinks (MCHS). This numerical study, conducted for Reynolds numbers between 1190 and 1900, was complemented by the fabrication of two models (a conventional model and an improved model). The comparison between experimental and numerical results showed good agreement, highlighting the superiority of the improved model in terms of thermal resistance and pressure drop. Moreover, Xin et al. [12] explored the optimization of the substrate temperature gradient in a serpentine MCHS. By experimentally and numerically comparing a double-serpentine heat sink, they analyzed three inlet-outlet configurations. Their results showed that increasing the number of holes in the channel walls improved the average Nusselt number by 26%, effectively reducing the substrate temperature. Al-Hasani and Freegah [13] conducted a numerical and experimental study on the hydrothermal performance of three serpentine MCHS configurations. Two new models (A and B) were compared with a conventional model. Model A featured a central inlet and two lateral outlets, while Model B had a single inlet that split before reaching two outlets on the same side. The results showed an improvement in the thermal performance of models A and B compared to the conventional heat sink, with a notable advantage for Model B in terms of temperature distribution, Nusselt number, base temperature, and thermal resistance. Moreover, in another study, Al-Hasani and Freegah [14] investigated performance enhancement in a serpentine MCHS by testing several configurations: double outlet, secondary flow at different angles (45°, 53°, 61°), and secondary flow with fins. The experimental study validated numerically, revealed that adding an outlet improved overall performance by a factor of 1.47 while reducing the maximum temperature. The integration of fins with secondary flow also optimized thermal and hydraulic performance.

Although many studies have explored serpentine mini-channel heat sinks, certain areas remain underexplored and require further investigation. In response to these gaps, this study examines four novel serpentine mini-channel heat sink designs aimed at enhancing thermal performance. Copolymer resin was selected for model fabrication due to its lightweight nature and insulating properties - a material choice that is rarely emphasized in heat sink research. The study systematically analyzes key performance indicators such as pressure drop, thermal resistance, average Nusselt number, flow rates, average temperature, and coolant properties to achieve a well-rounded improvement in overall heat sink efficiency.

COMPUTATIONAL AND NUMERICAL METHODS

Proposed serpentine minichannel heat sink inlet /outlet positions

Figure 1 illustrates a 3D configuration of a serpentine minichannel heat sink (MCHS), designed to cool electronic components by circulating a heat transfer fluid through the minichannel. Table 1 illustrates the system's dimensions.
The cooler consists of two main parts: the upper section (the cover), made of copolymer resin, and the lower section, made of aluminum, which serves as the thermal dissipation component. A constant thermal flux was applied to the lower wall of the heat sink, which is treated as an electronic component generating heat. Water, used as the heat transfer fluid, enters through the minichannel inlet and exits through the outlet.

Four distinct configurations, shown in Figure 2, were analyzed. These configurations involve different arrangements of fluid inlet and outlet, allowing an assessment of their impact on the thermal performance of the heat sink. The fluid inlet temperature is maintained at a constant 293 K throughout the study. The properties of the materials and fluid used are detailed in Table 2.

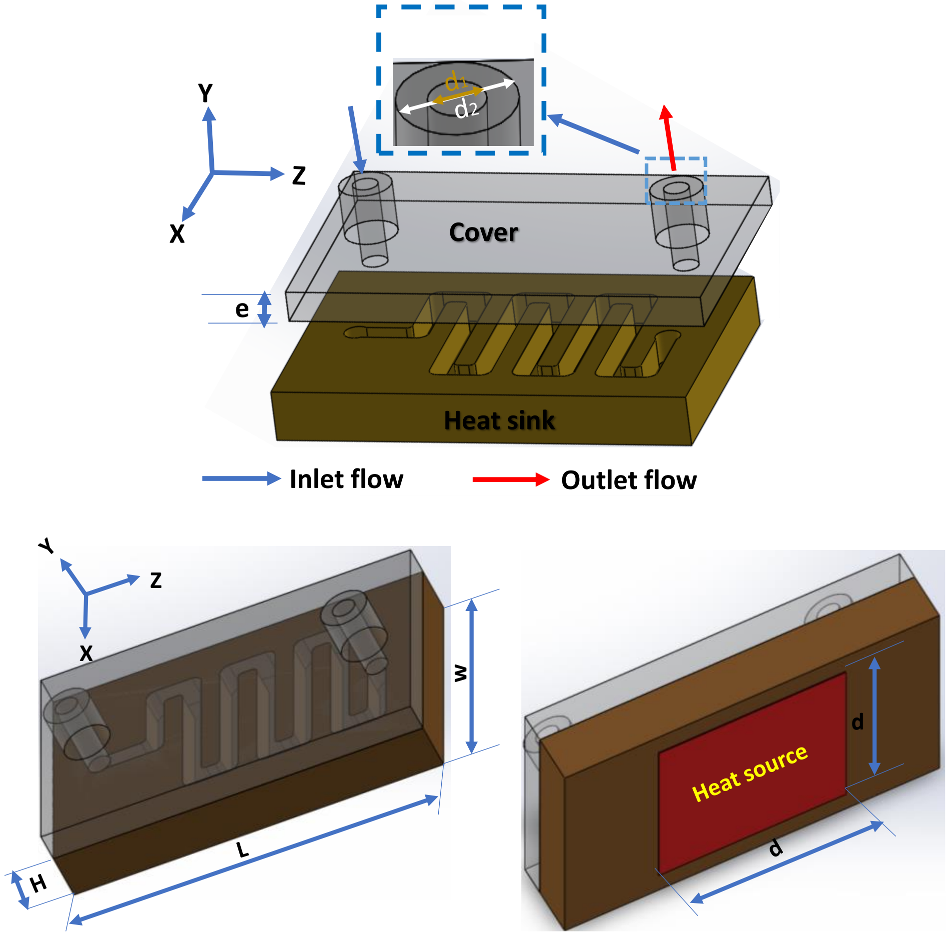

Fig. 1. Design of the three-dimensional configuration considered

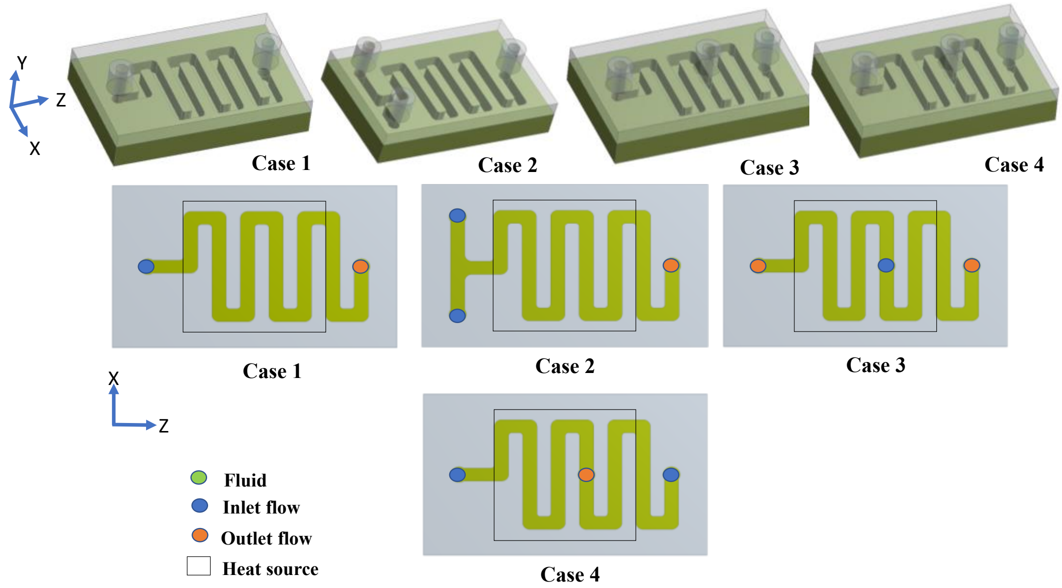

Fig. 2. Schematic configurations of the cases used

The four models investigated are as follows:

a) The first model incorporates a serpentine minichannel heat sink, featuring a single inlet and outlet for the coolant.
b) The second model is designed with two coolant inlets and a single outlet.
c) The third model includes one inlet and two outlets.
d) The fourth model is similar to the third, with the only distinction being the reversal of the inlet and outlet positions for the coolant.

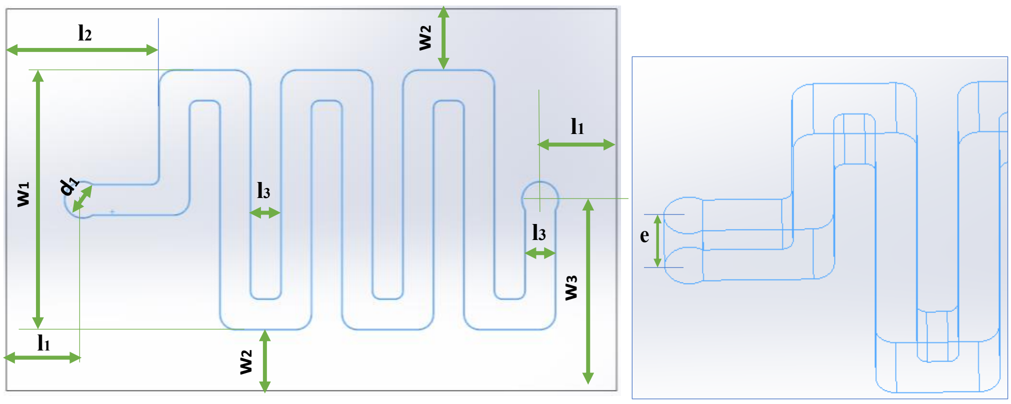

Fig. 3. Heat sink dimension

Table 1. *Dimensions of the heat sink (Dimensions in mm)*

	L	H	W	d	d_1	d_2	l_1	l_2	l_3	w_1	w_2	w_3	e
Allcases	40	5	25	20	2.4	5	5	10	2	17	4	12.5	3

Table 2. *Thermophysical properties of water, aluminum and copolymer resin [15]*

	ρ (kg/m^3)	Cp ($J/kg.K$)	k (W/mK)	μ ($kg/m\cdot s$)
Water	998.2	4182	0.613	0.001003
Aluminum	2719	871	202.4	---
ABS copolymer resin	1040	800	0.17	---

Where μ, ρ, k and C_p are the dynamic viscosity of coolant, the density, the thermal conductivity and the specific heat, respectively.

Boundary conditions and mathematical equations

To solve the equations governing the natural convection of a viscous fluid, several assumptions were made to simplify the analysis of the phenomenon. First, two types of flow are considered in this study: laminar flow, characterized by a regular and stable motion, and steady flow, where the flow properties remain constant over time.

The fluid used in this study was assumed to be incompressible, meaning its density remains constant throughout the flow. Furthermore, it is treated as a Newtonian fluid, meaning its viscosity is considered constant and does not vary with flow velocity.

Additionally, certain effects such as the Joule effect and viscous dissipation are considered negligible and are not accounted for in the analysis. Finally, the physical properties of the fluid, including viscosity and density, are assumed to remain invariant throughout the entire flow process.

At the inlet (Case 1): The velocity components along the x-axis, y-axis, and z-axis are set to $u = v = 0$; the velocity component along the z-axis is set to $w = w_{in1}$ = constant. The temperature at the inlet is fixed at $T = T_{in}$ =293 K

At the inlet (Case 2 and Case 4): Similarly, the velocity components are $u = v = 0$, and the velocity along the z-axis is set to $w = w_{in2}$ = constant. The temperature is maintained at $T = T_{in2}$ = 293 K

At the outlet: The gauge pressure is set to $P = 0$.

At the mini-channel walls: The velocity components (u, v, w) are set to 0, and the temperature is specified as $T=T_{wall}$

At the bottom wall of the heat sink: A constant heat flux Q is applied.

Formula No. 1: This formula is applied at the fluid-solid interface to ensure the continuity of heat flux between the solid and the fluid.

$$k_{Solid}\frac{\partial T}{\partial n}\bigg| wall = k_{water}\frac{\partial T}{\partial n}\bigg| wall \tag{1}$$

Each microchannel wall is subjected to no-slip boundary conditions.

The mass conservation equation (2), the momentum equations (3, 4, 5), the energy conservation equation (6), and the solid equation (7) were applied using the finite volume method [16].

The formulation of the mass conservation equation is expressed as:

$$\frac{\partial u}{\partial x}+\frac{\partial v}{\partial y}+\frac{\partial w}{\partial z}=0 \tag{2}$$

The form of the momentum equations are as follows:

Along the x-axis

$$u\frac{\partial u}{\partial x}+v\frac{\partial u}{\partial y}+w\frac{\partial u}{\partial z}=\frac{1}{\rho_{water}}\left[-\frac{\partial P}{\partial x}+\mu_{water}\left(\frac{\partial^2 u}{\partial x^2}+\frac{\partial^2 u}{\partial y^2}+\frac{\partial^2 u}{\partial z^2}\right)\right] \tag{3}$$

Along the y-axis

$$u\frac{\partial v}{\partial x}+v\frac{\partial v}{\partial y}+w\frac{\partial v}{\partial z}=\frac{1}{\rho_{water}}\left[-\frac{\partial P}{\partial y}+\mu_{water}\left(\frac{\partial^2 v}{\partial x^2}+\frac{\partial^2 v}{\partial y^2}+\frac{\partial^2 v}{\partial z^2}\right)\right] \tag{4}$$

Along the z-axis

$$u\frac{\partial w}{\partial x}+v\frac{\partial w}{\partial y}+w\frac{\partial w}{\partial z}=\frac{1}{\rho_{water}}\left[-\frac{\partial P}{\partial z}+\mu_{water}\left(\frac{\partial^2 w}{\partial x^2}+\frac{\partial^2 w}{\partial y^2}+\frac{\partial^2 w}{\partial z^2}\right)\right] \tag{5}$$

where μ_{water}, ρ_{water} and P are the dynamic viscosity and the density of the water, and the pressure, respectively.

The energy equation is:

$$u\frac{\partial T}{\partial x}+v\frac{\partial T}{\partial y}+w\frac{\partial T}{\partial z}=\alpha_{water}\left(\frac{\partial^2 T}{\partial x^2}+\frac{\partial^2 T}{\partial y^2}+\frac{\partial^2 T}{\partial z^2}\right) \tag{6}$$

where $\alpha_{water}$and T are the thermal diffusivity and the temperature of the water, respectively.

To describe heat transfer through a solid wall, equation N°7 is applied:

$$\frac{\partial^2 T_s}{\partial x^2}+\frac{\partial^2 T_s}{\partial y^2}+\frac{\partial^2 T_s}{\partial z^2}=0 \tag{7}$$

where T_s is solid temperature.

The average Nusselt number (Nu_{ave}) is calculated using the following formula [16]:

$$Nu_{ave}=\frac{h_{av}\,D_h}{k} \tag{8}$$

where D_h is the hydraulic diameter.

$$h_{av}=\frac{Q}{A_w\left(T_w-T_f\right)} \tag{9}$$

where T_w, T_f, k, A_w are the average temperature of the wall, the average temperature of water, the liquid thermal conductivity and the convection heat transfer area, respectively.

$$D_h=\mathrm{d}_1=\frac{4\times \mathrm{e}\times \mathrm{l}_3}{2\,(\mathrm{e}+\mathrm{l}_3)}(10)$$

The pressure drop is calculated from the following formula:

$$\Delta P = P_{in}–P_{out} \tag{11}$$

Improving heat transfer through passive techniques is often linked to an increase in pressure (ΔP). To assess the effectiveness of these approaches, the Performance Evaluation Factor (PEF).

The performance evaluation factor is calculated by [17]:

$$PEF = \frac{f_{Nu}}{f_{\Delta P}{}^{1/3}} \tag{12}$$

$$f_{Nu} = \frac{Nu_{ave}}{Nu_{ave,\ case\ 1}} \quad ; \quad f_{\Delta p} = \frac{\Delta P}{\Delta P_{case\ 1}}$$

where ΔP_{case1} and $Nu_{ave,case1}$ are the pressure drop and the average Nusselt number of the 1st case, respectively.

The formulation of the thermal resistance is expressed as:

$$R_{th} = \frac{T_{max} - T_{in}}{Q} \tag{13}$$

Where T_{max} and T_{in} are the maximum temperature on the bottom wall and the inlet temperature of the water, respectively.

Independent Mesh analysis

Tetrahedral mesh was selected and used in this study, see Figure 4. An increased number of nodes was used at the interfaces between the coolant fluid surface and the channel walls, as these areas are crucial for heat transfer. Figures 5a and b show the impact of the mesh on the numerical results and determine the number of nodes ensuring the stability of the results.

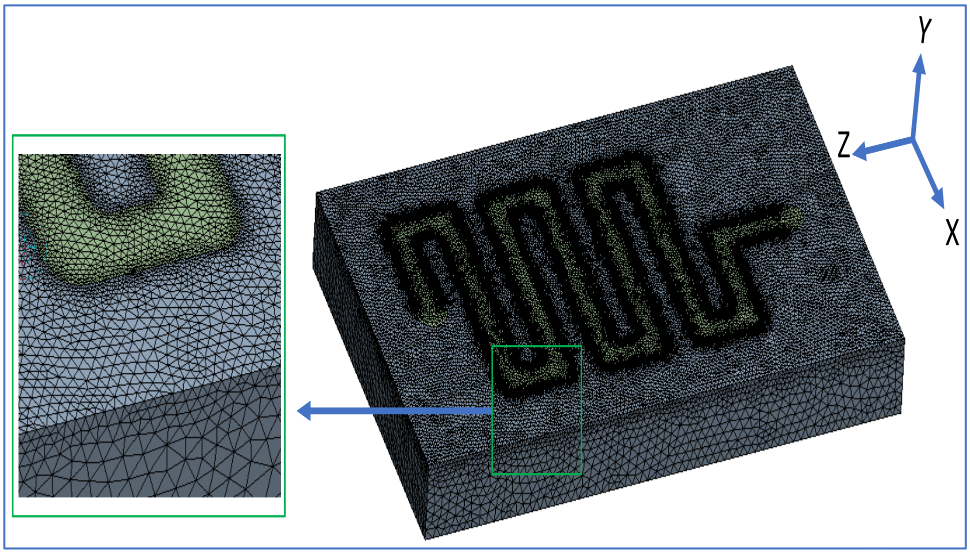

Fig. 4. Mesh distribution in the model.

To investigate the influence of the mesh on key parameters such as the average Nusselt number, pressure drop, and the average temperature of the heat source. The Reynolds number was set at 300, and water was chosen as the coolant. The results showed that for a mesh of 61,030 to 105,814 nodes, a variation of 44,784 nodes led to changes of 0.104 in the average Nusselt number, 2.73 Pa for the pressure drop, and 0.645 K for the average temperature of the heat source. However, when the number of nodes was increased from 240,800 to 1,568,549 nodes (a difference of 1,327,749 nodes), the variations became negligible, with changes of 0.05 for the average Nusselt number, 0.16 Pa for the pressure drop, and 0.17 K for the temperature. Hence, the results indicate that beyond a certain threshold of nodes, the variations become insignificant, thereby ensuring the accuracy of the simulation and the stability of the numerical results.

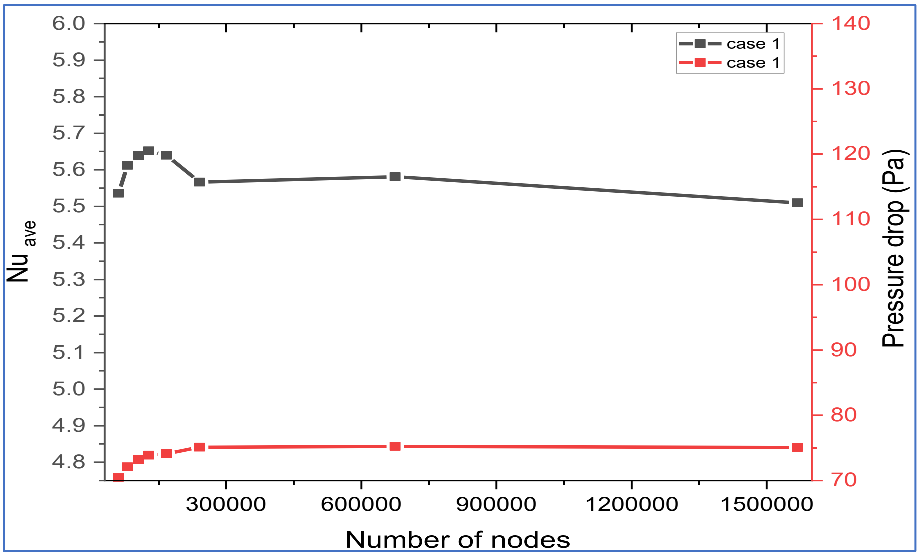

(a)

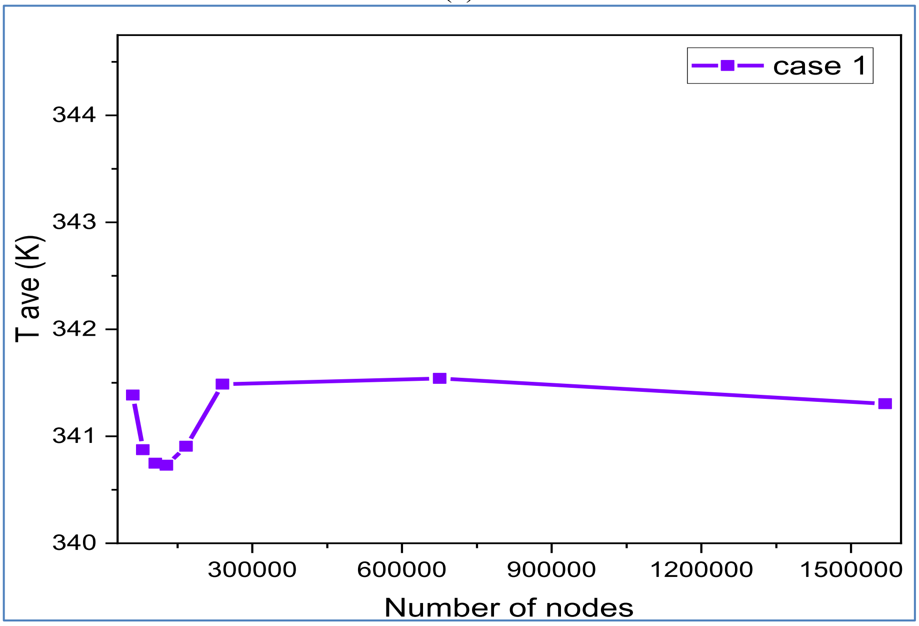

(b)

Fig. 5. Effect of the mesh on (a) pressure drop and the average Nusselt number, (b) the average temperature values of the heat source for case 1 at *Re* = 300

RESULTS AND DISCUSSIONS

Temperature distribution

Figure 6 illustrates the temperature distribution lines on the bottom surface of the heat sink for the four cases studied, at Reynolds numbers 200, 400, and 600. It can be observed that the maximum temperature is concentrated at the location of the heat source in all cases and for all Reynolds numbers.

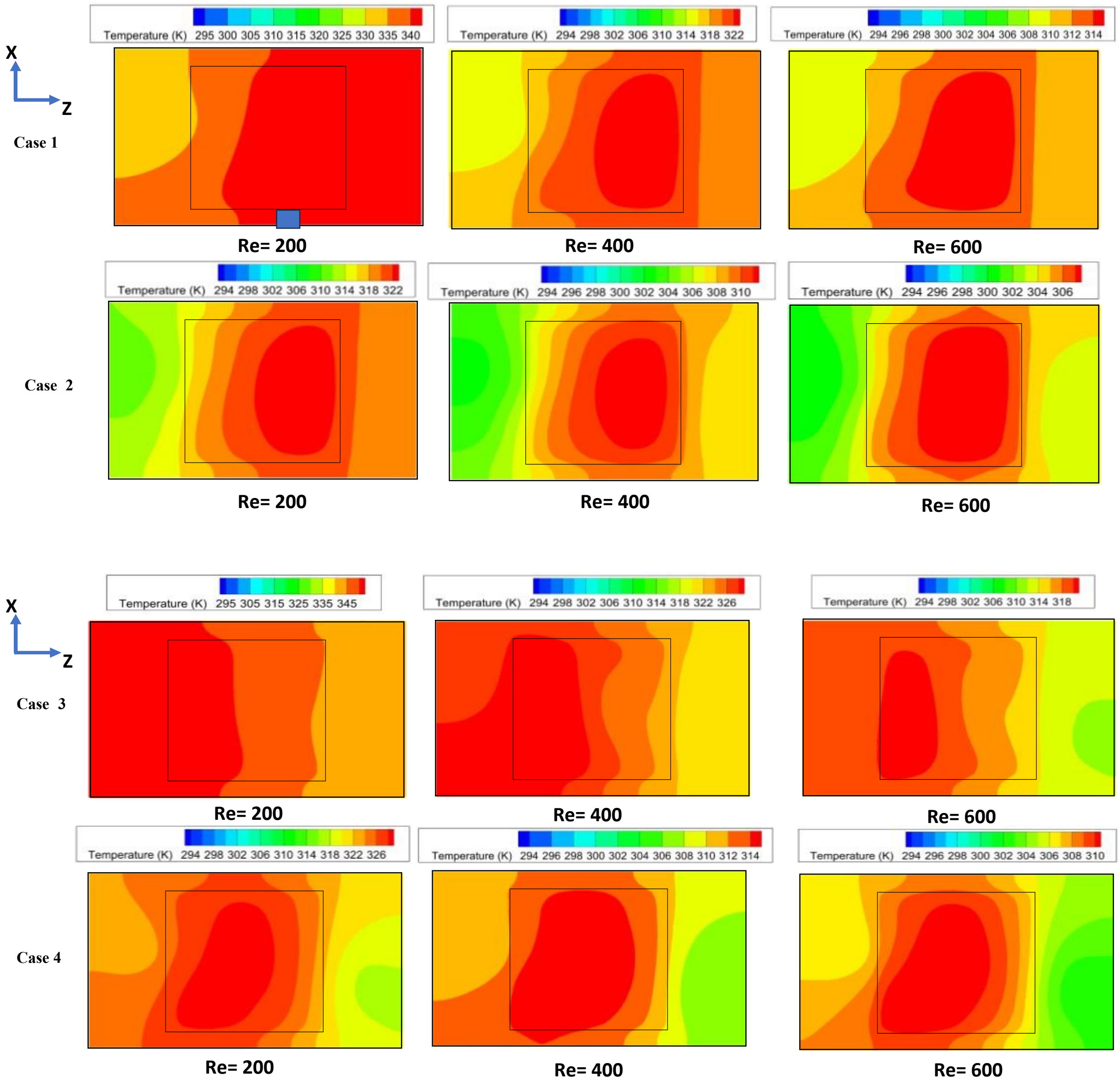

Fig. 6. Temperature distribution on the bottom wall for four cases with variable Reynolds numbers

Additionally, as the Reynolds number increases, the temperature lines change. The lowest temperature values tend to concentrate at the points where the coolant enters. Furthermore, the temperature values on the bottom surface of the wall decrease with the increase in the Reynolds number in all cases. For example, at a Reynolds number of 200, the temperature variation range in the four cases is approximately as follows: 330 to 340 K, 318 to 322 K, 340 to 350 K, and 318 to 328 K, respectively. In comparison, at a Reynolds number of 600, the temperature variations are as follows: 310 to 314 K, 304 to 307 K, 312 to 320 K, and 303 to 310 K.

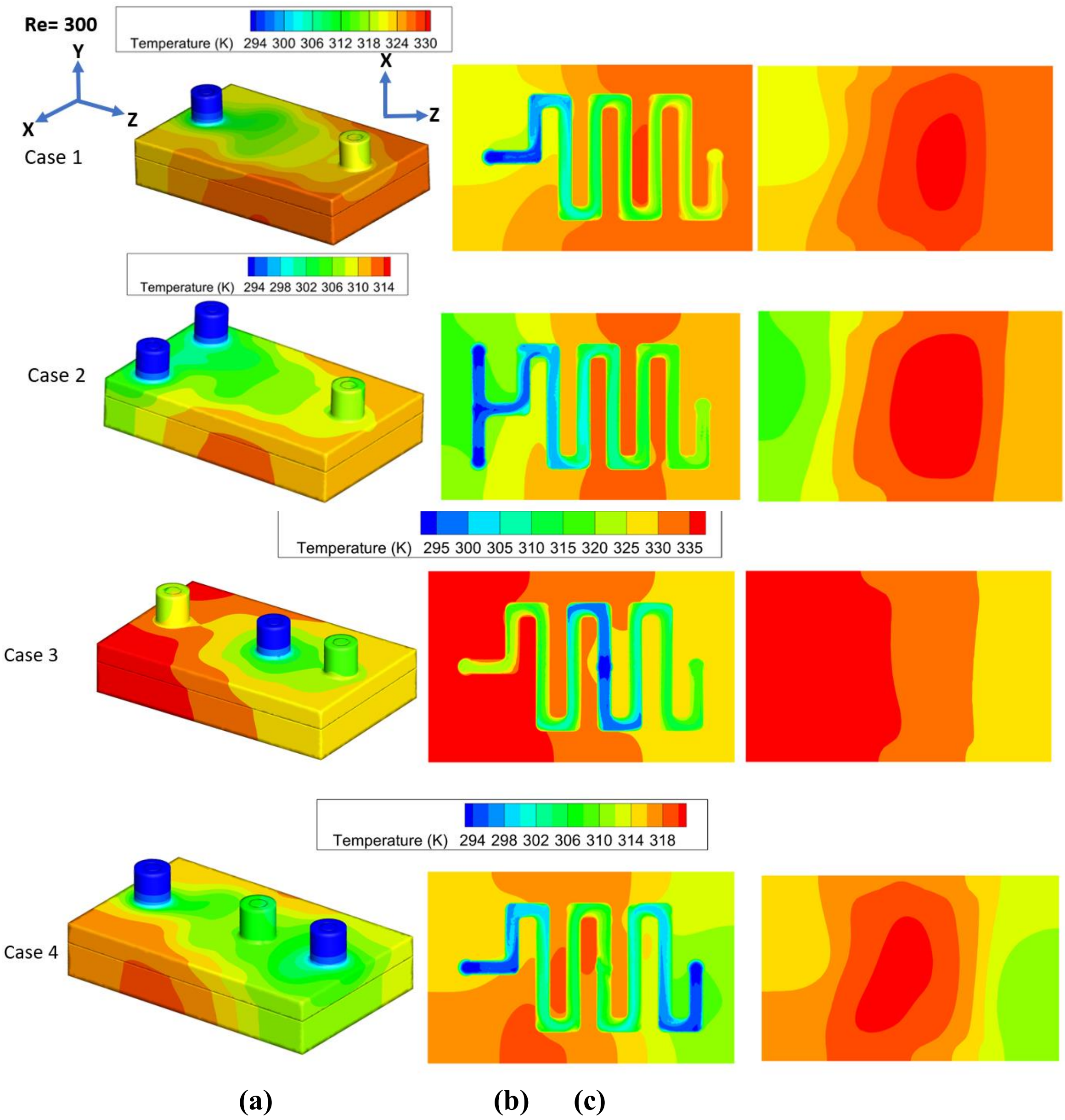

Fig. 7. (a) Temperature distribution in 3D (b) Temperature distribution at a height of h = 3.5 mm from the bottom wall of the heat sink (c)Temperature distribution on the bottom wall for four cases with *Re* = 300

Figure 7 presents the temperature profiles in both the liquid and solid domains for four models (see Figure 7a) under a constant heat flux of 150,000 W/m² and a Reynolds number of 300 across all four cases. The obtained results demonstrate that the position of the inlet and outlet of the coolant significantly influences the shape of the temperature curves in each case, as clearly illustrated in Figure 7a. The highest temperature is observed in case 3, reaching approximately 334 K. Case 1 follows with a slightly lower temperature of 331 K. Conversely, cases 4 and 2 show considerably lower temperatures of 320 K and 315 K, respectively, highlighting the thermal performance differences among the configurations.

In contrast, Figure 7b shows that the temperature difference between the inlet and outlet of the coolant in each case is linked to the configuration of the minichannel and the positioning of the inlet and outlet. It can be observed that the coolant temperature gradually increases as the flow progresses toward the outlet, where the coolant gains heat from the hot heat sink channel. Furthermore, the intensity of heat transfer between the aluminum and water is maximal at the channel inlet in each case.

Moreover, the heat transfer between the narrow walls of the channel and the liquid has a significant impact on the lower wall of the heat sink in each case (see Figure 7c). This effect is highlighted by the evolution of the temperature profiles: the temperature values in the second and fourth cases are lower than those in the first and third cases. This indicates that the last two models offer better performance, likely due to faster thermal dissipation, contributing to improved thermal transfer efficiency.

Temperature variation of the heat source for four cases

Figure 8 shows the variation of the maximum and average temperatures of the heat source as a function of the Reynolds number for the four studied cases. Both the maximum and average temperatures of the heat source decrease with the increase in flow velocity in all four cases. Moreover, the second and fourth cases present lower values compared to the third and first cases. This is due to the presence of two inlet ports in the minichannel, which improves heat transfer between the water and the minichannel walls. This improvement increases with the Reynolds number (i.e., the increase in fluid inlet velocity into the channel). Furthermore, it is observed that the second case surpasses the fourth case in terms of reducing the average temperature. This is due to the difference in the positioning of the channel inlets. At Reynolds numbers 200 and 600, the temperature reduction is 25 and 13 Kelvin, respectively.

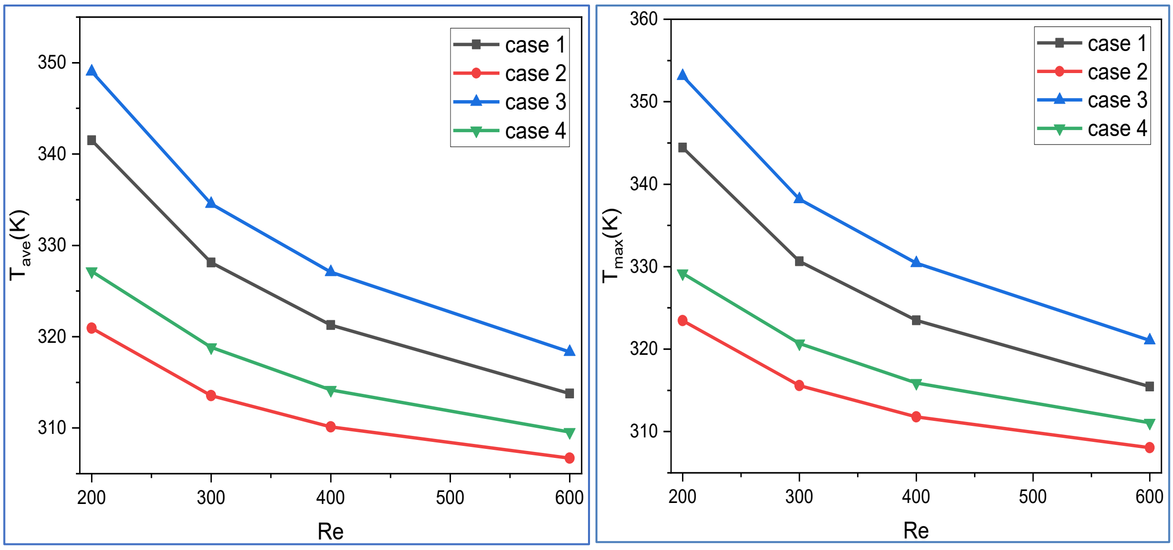

Fig. 8. Variation of T_{ave} and T_{max} on the heat source for Re between 200 and 600 across four cases

Nusselt number

Figure 9 illustrates the relationship between the average Nusselt number and fluid flow . The analysis of velocity for four different heat sink configurations, as the Reynolds number increases from 200 to 600, reveals key trends in heat transfer performance. The results indicate that as flow velocity increases, the average Nusselt number rises across all cases. Notably, the heat sinks in the fourth and second cases exhibit higher average Nusselt numbers compared to those in the first and third cases, highlighting improved heat transfer efficiency.

Furthermore, the difference in the average Nusselt number between the four cases becomes more pronounced with increasing flow velocity. For instance, as the Reynolds number rises from 200 to 600, the variation in the Nusselt number between the cases becomes significantly more distinct. Specifically, in the first case, the difference increases by a factor of 8.34, in the second case by 11.56, in the third case by 6.42, and in the fourth case by 10.48.

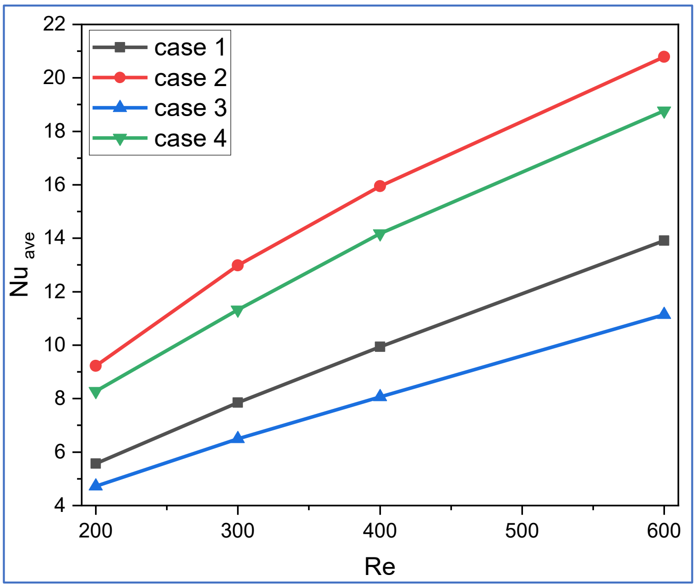

Fig. 9. Nu_{ave} for *Re* ranging from 200 to 600 across four cases

Additionally, at a Reynolds number of 600, the discrepancy in the average Nusselt number compared to the third case is considerable: it is 2.76 times higher in the first case, 9.65 times higher in the second case, and 7.62 times higher in the fourth case. These variations emphasize the influence of inlet and outlet configurations on heat transfer performance, with the second and fourth cases demonstrating superior thermal efficiency.

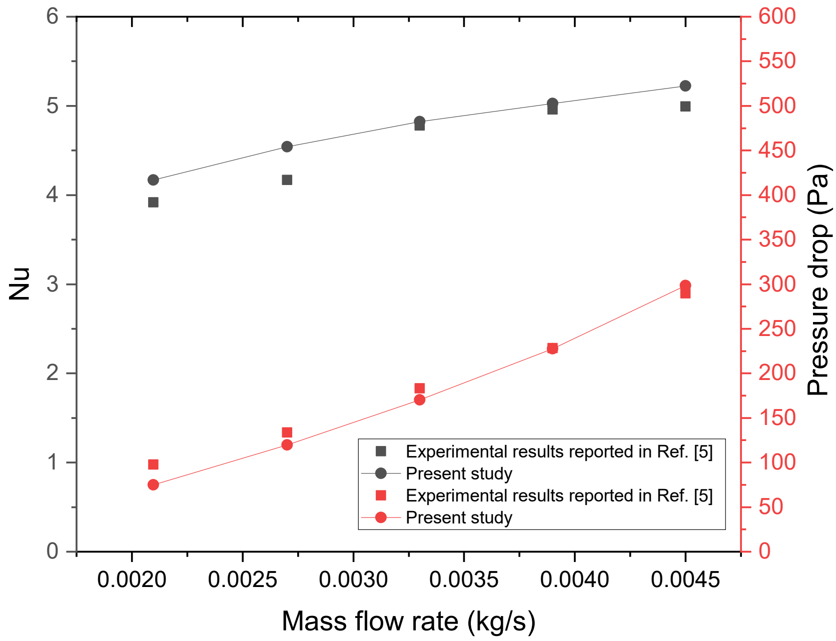

Fig. 10. Variation of the Nusselt number and pressure drop as a function of flow rate

Figure 10 shows the variations of the pressure drop (shown in red color) and the average Nusselt number (shown in black color) for the minichannel heat sink studied in Ref. [5], as a function of the mass flow rate of coolant (water), ranging from 0.0021 to 0.0045 kg/s. The results indicate that as the flow rate of the coolant increases, both the average Nusselt number and the pressure drop within the mini channels also increase. This behavior is attributed to the higher flow velocity, which leads to increased pressure and enhanced thermal transfer within the mini channel. Additionally, Figure 6 compares the numerical results with experimental data from other researchers [5]. The figure shows a certain degree of agreement between the numerical results and those reported in reference [5], confirming the accuracy of the simulation and the validity of the obtained results. However, some discrepancies in the Nusselt number values are observed, with the maximum difference between the experimental and numerical values reaching approximately 0.372, while the smallest difference is around 0.045. Regarding the pressure drop values, the results indicate agreement between the numerical data and the experimental data.

Flow behavior and characteristics

Figure 11 shows the flow velocity distribution in four different serpentine mini-channel heat sink configurations at a Reynolds number of 300, measured at a height of 3.5 mm from the bottom wall. The results highlight distinct flow behaviors that influence both pressure drop and heat transfer efficiency.

In the second case, the highest flow velocities are observed at the channel bends, leading to an increase in pressure drop (as shown in Figure 12) while improving heat transfer (as shown in Figure 9). The maximum velocity reaches 0.33 m/s, which is attributed to the specific positioning of the fluid inlets. In contrast, in the first and fourth cases, the flow velocities are lower than in the second case, remaining close to the inlet velocity, around 0.175 m/s and 0.178 m/s, respectively.

In the third case, the maximum velocity is concentrated at the fluid inlet, while it remains nearly constant along the middle of the channel. This suggests less efficient heat transfer due to the configuration of the fluid inlets and outlets, which also results in a lower pressure drop within the channel. Consequently, the third case exhibits the lowest pressure drop values among all configurations, as confirmed by Figure 12.

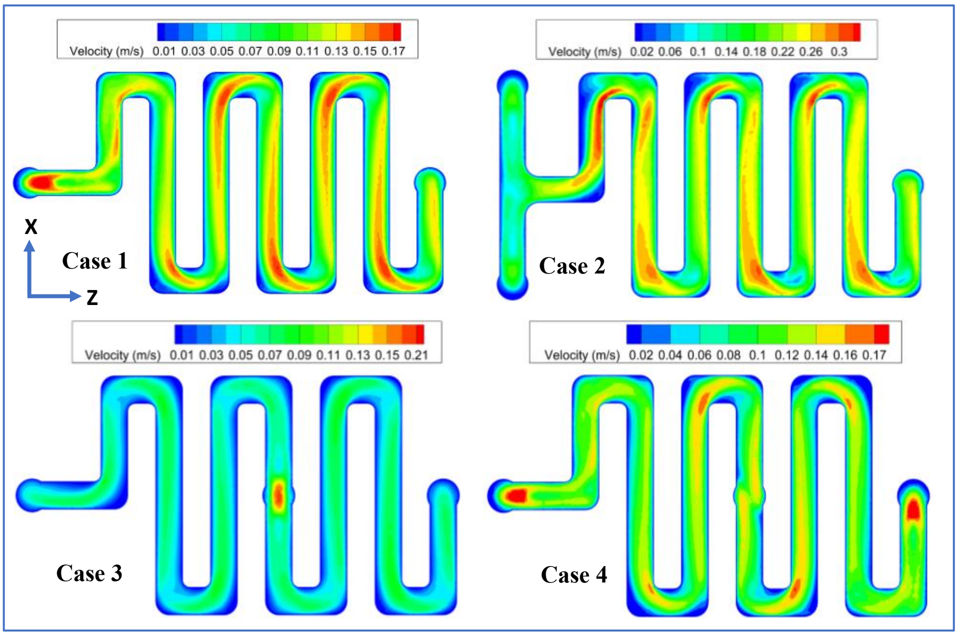

Fig. 11. Flow velocity distribution in the minichannel at a height of 3.5 mm

Pressure drop

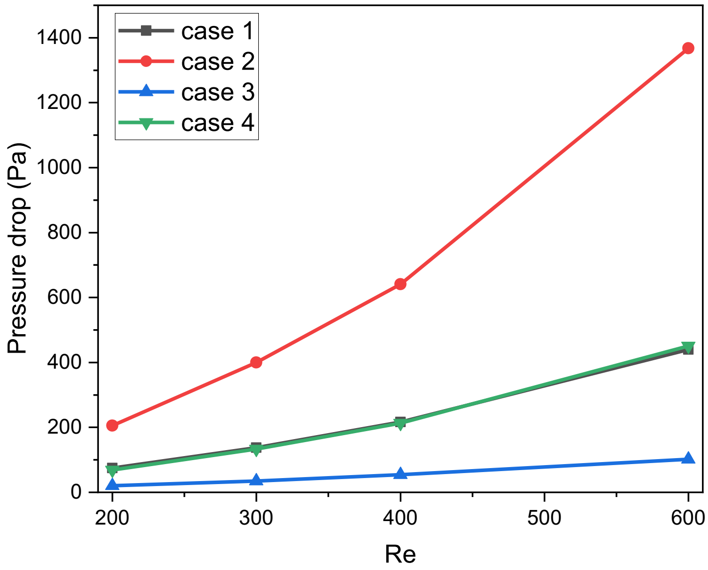

Fig. 12. Pressure drop as a function of *Re* for all cases studied

Figure 12 illustrates the effect of the Reynolds number on flow velocity and its influence on pressure drop for the four cases studied. Based on the results obtained, it can be concluded that an increase in flow velocity generally leads to an increase in pressure drop across all four cases.

Further analysis shows that the second case exhibits a high flow friction force, resulting in a more significant pressure drop compared to the other cases, especially as the flow velocity increases. This indicates that the interaction between the flow and the surfaces leads to greater resistance, causing a noticeable pressure drop. In contrast, the pressure drop values in the first and fourth cases are quite similar and, in some instances, identical, despite their thermal performances not being the same. This suggests that the fourth case model is more efficient than the second case model, as it shows lower pressure drop values, making its design more effective. As for the third case, although it demonstrates lower pressure drop values, its thermal performance is weak compared to the other cases. Therefore, despite the lower pressure drop, its poor thermal performance reduces the overall effectiveness of this model.

Thermal resistance

Figure 13 illustrates the relationship between thermal resistance and the Reynolds number of the heat sink for four different cases. The results show that thermal resistance decreases with increasing flow velocity across all four cases. Specifically, the thermal resistance values for the fourth case are 0.56, 0.43, 0.35, and 0.27 K/W for Reynolds numbers 200, 400, 300, and 600, respectively. These results align with those obtained by other researchers [18].

Additionally, the results indicate that within the Reynolds number range of 200 to 600, the second case exhibits the lowest thermal resistance values compared to the other cases, suggesting that it significantly contributes to the improvement of heat transfer. In contrast, the third case shows higher thermal resistance values, indicating that the heat sink cannot effectively distribute heat. For the first and fourth cases, the thermal resistance values at the highest Reynolds number are 0.346 K/W and 0.276 K/W, respectively, reflecting a different heat transfer behavior compared to the other cases.

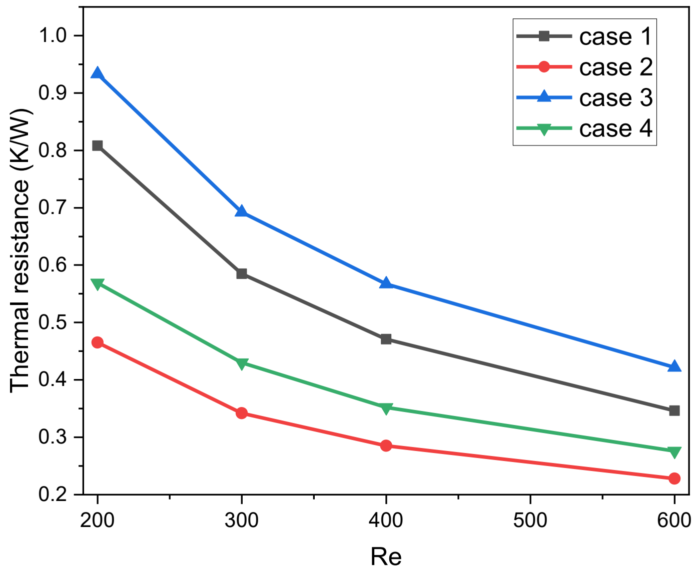

Fig. 13. Thermal resistance (R_{th}) as a function of Reynolds number (*Re*)

The performance evaluation factor (PEF)

Figure 14 illustrates the variation in the Performance Evaluation factor (PEF) for the second, third, and fourth configurations within a Reynolds number range of 200 to 600. A decreasing trend in PEF is observed across all three cases as the Reynolds number increases, primarily due to the rise in pressure drop at higher Reynolds numbers.

The figure also highlights the positive effect of incorporating two fluid inlets in the fourth configuration, which enhances the heatsink performance. Although the second configuration achieves a higher Nusselt number compared to the fourth (as shown in Figure 9), its PEF value is lower due to the significantly higher-pressure drop associated with this case.

On the other hand, the first configuration, characterized by a low-pressure drop, offers an overall improved performance. At a Reynolds number of 200, the PEF values were approximately 1.189 for the second case, 1.31 for the third, while the fourth configuration exhibited the highest performance with a PEF of 1.531.

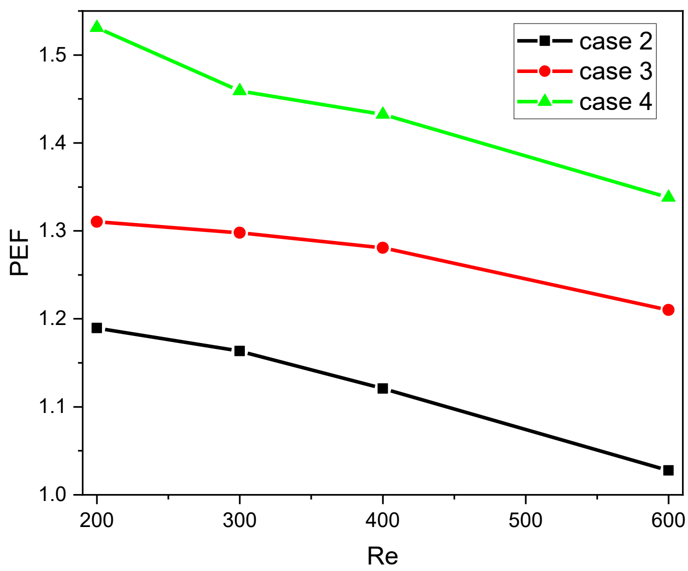

Fig. 14. *PEF variation* with Reynolds number (*Re*) for four different cases

Impact of inlet and outer flow positions on T_{ave} and Nu_{ave}

Figure 15 shows the impact of the fluid inlet and outlet locations in the third and fourth cases. The investigations focus on figuring out how modifications to the fluid inlet and outlet points affect the system's behavior, including the potential impacts on the Nusselt number (Nu_{ave}) and the average temperature (T_{ave}).

To investigate this, we selected three different positions for the fluid inlet while keeping the outlet fixed in the third case. Conversely, in the fourth case, we chose three different positions for the fluid outlet while keeping the inlet fixed.

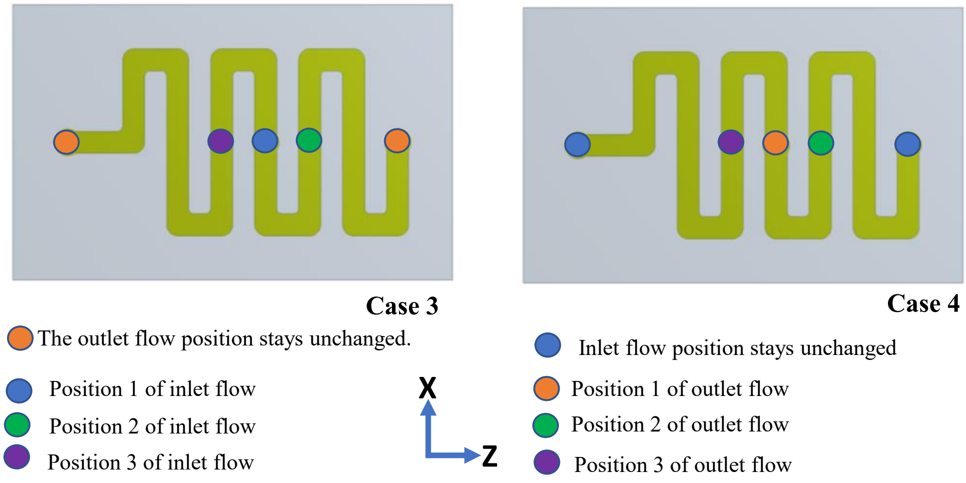

Fig. 15. Flow positions in the third and fourth cases

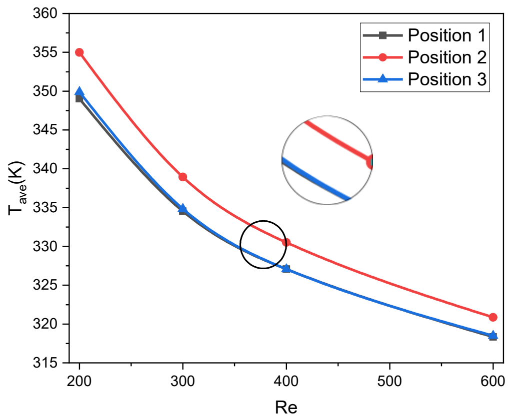

Fig. 16. Effect of inlet flow position in case 3 on T_{ave}

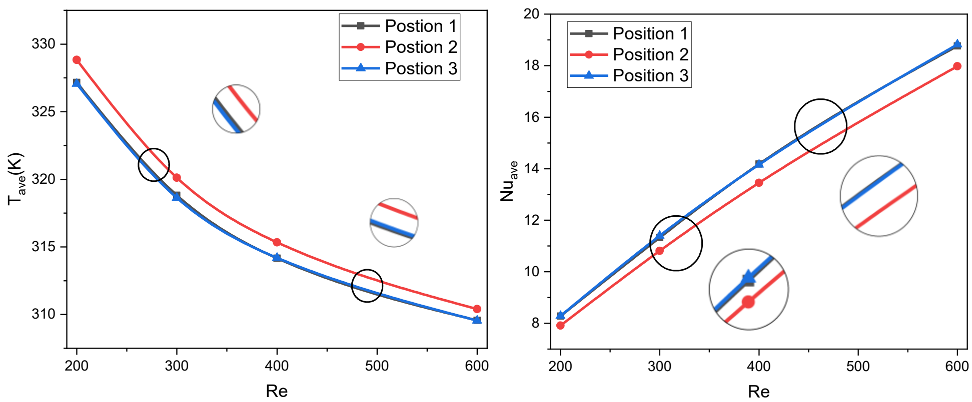

Fig. 17. Effect of outlet flow position in case 4 on T_{ave} and Nu_{ave}

Figure 16 illustrates the effect of the fluid inlet position on the average temperature in the third case for Reynolds numbers between 200 and 600. According to the results in Figure 16, the impact is particularly significant at position 2, where the average temperature of the heat source is higher than at positions 1 and 3, and it remains elevated for all Reynolds numbers between 200 and 600. This is attributed to the reduced heat exchange between the channel walls and the fluid.

In contrast, positions 1 and 3 have a similar effect on the average temperature of the heat source due to their placement near the centre of the heat sink, which contributes to more efficient thermal distribution. A similar observation is noted when the inlet and outlet positions of the fluid are reversed, as shown in Figure 17, which illustrates the impact of the fluid outlet position on the average temperature and the heat exchange efficiency in the fourth case. Position 2 leads to a significant increase in the average temperature of the heat source, thereby reducing the efficiency of the heat sink in both the third and fourth cases.

CONCLUSIONS

In the context of enhancing the thermal efficiency of a cooler equipped with an aluminum heat sink with a cover of polymer resin material, this study investigates the impact of coolant inlet and outlet design on the heat transfer characteristics of a serpentine mini-channel heat sink. Four different configurations were examined within a Reynolds number range of 200 to 600. Numerical analysis was employed to evaluate and compare the performance of the proposed designs. Based on the findings of the current study, several key conclusions were drawn.

− Cases 2 and 4 (two-inlet, one-outlet) provided the best thermal performance, showing lower thermal resistance and heat source temperatures.
− Case 3 (one-inlet, two-outlet) had the poorest thermal efficiency despite lower pressure drop.
− Case 2 achieved the lowest thermal resistance (0.228 K/W), while Case 4 showed the best Performance Evaluation factor (*PEF*)value (1.531) at Re = 200.
− Thermal performance improved with increasing flow velocity in all cases, as reflected in higher average Nusselt numbers and reduced heat source temperatures.
− Inlet/outlet configuration significantly affects thermal efficiency, with a trade-off between heat transfer and pressure drop.

ACKNOWLEDGEMENTS

The authors would like to express their sincere gratitude to the Ministry of Higher Education and Scientific Research of Algeria for its generous funding and continuous support of this study. Great thanks are also extended to the collaborating institutions for their valuable support and contributions: the Research Centre in Industrial Technologies (CRTI), Abbas Laghrour University of Khenchela, Laboratory of Materials and Energy Engineering, LGEM, University of Mohamed Khider Biskra, Eco-Materials, Chemical Processes and Sustainable Development Laboratory, University of Mohamed Khider Biskra, Algeria, ITheMM - Institut de Thermique, Mécanique, Matériaux, Université de Reims Champagne-Ardenne, France; and the School of Engineering and Sustainable Development, De Montfort University, United Kingdom.

REFERENCES

1. Imran, A. A., Mahmoud, N. S., Jaffal, H. M., “Numerical and experimental investigation of heat transfer in liquid cooling serpentine mini-channel heat sink with different new configuration models,” Thermal Science and Engineering Progress, Vol. 6, pp. 128-139, 2018. https://doi.org/10.1016/j.tsep.2018.03.011.
2. Tariq, H.A., Anwar, M., Malik, A., "Numerical investigations of mini-channel heat sink for microprocessor cooling: effect of slab thickness". Arab J Sci Eng 45, pp.5169-5177, 2020. https://doi.org/10.1007/s13369-020-04370-4
3. Ghadhban, F. N., Hayder M. J., "Numerical and experimental thermohydraulic performance evaluation of multi-minichannel heat sinks considering channel structure modification," International Communications in Heat and Mass Transfer, Vol. 145, Part A, 106847, 2023, https://doi.org/10.1016/j.icheatmasstransfer.2023.106847.
4. Chadi, K., Belghar, N., Lachi, M., Driss, Z., Bencid, A. "Numerical study of the optimization of the thermal and flow characteristics of a collector design of microchannels with two inlets and outlets, containing a nanofluid and a water-based fluid". Numerical Heat Transfer, Part A: Applications, pp.1-15,2024.https://doi.org/10.1080/10407782.2024.2357586
5. Mahmoud, N. S., Jaffal, S. M., Imran, A. A., "Performance evaluation of serpentine and multi-channel heat sinks based on energy and exergy analyses," Applied Thermal Engineering, Vol. 186, 116475, 2021.https://doi.org/10.1016/j.applthermaleng.2020.116475.
6. Gorzin, M., Ranjbar, A.A., Hosseini, M.J., "Experimental study on serpentine minichannel heat sink: Effect of rib existence and distance," International Journal of Thermal Sciences, Vol. 173, 107397,2022. https://doi.org/10.1016/j.ijthermalsci.2021.107397
7. Mustafa, A.J., Ihsan A.G., " Performance analysis of minichannel heat sink with oblong cavities and diverse pin fin configurations."Heat transfer, Vol. 54, Issue1, pp. 854-882, 2025 https://doi.org/10.1002/htj.23198
8. Afshari, F., Muratçobanoğlu, B., "Thermal analysis of Fe_3O_4/water nanofluid in spiral and serpentine mini channels by using experimental and theoretical models". Int. J. Environ. Sci. Technol. 20, pp.2037-2052, 2023.https://doi.org/10.1007/s13762-022-04119-6
9. Ataei, M., Sadegh Moghanlou, F., Noorzadeh, S., Vajdi, M., Shahedi Asl, M., "Heat transfer and flow characteristics of hybrid Al_2O_3/TiO_2–water nanofluid in a minichannel heat sink". Heat Mass Transfer 56, pp. 2757-2767, 2020. https://doi.org/10.1007/s00231-020-02896-9
10. Saleem, S., Heidarshenas, B., "An investigation on exergy in a wavy wall microchannel heat sink by using various nanoparticles in fluid flow: two-phase numerical study". J Therm Anal Calorim 145, pp.1599-1610, 2021. https://doi.org/10.1007/s10973-021-10771-w
11. Mahmood, H., Freegah, B., Muneer EL-Deen Faik, A., Qasim, S., "Optimizing minichannel heat sink design: A combined numerical and experimental analysis of Inlet/Outlet configurations and pin fin enhancements" Heat Transfer, 2024. https://doi.org/10.1002/htj.23267
12. Xin C., Huan-ling L., Xiao-dong S., Han S., Gongnan X.,"Thermal performance of double serpentine minichannel heat sinks: Effects of inlet-outlet arrangements and through-holes.", International Journal of Heat and Mass Transfer, Vol. 153, 119575, 2020, https://doi.org/10.1016/j.ijheatmasstransfer.2020.119575.
13. Al-Hasani, H. M., Freegah, B.," Influence of fluid inlet–outlet on hydrothermal evaluation for different serpentine mini-channel heat sink configurations", Heat Transfer, Vol. 51, Issue 8, pp. 7635-7654, 2022.https://doi.org/10.1002/htj.22659
14. Al-Hasani, H. M., Freegah, B., "Influence of secondary flow angle and pin fin on hydro-thermal evaluation of double outlet serpentine mini-channel heat sink", Results in Engineering, Vol. 16, 100670, 2022.https://doi.org/10.1016/j.rineng.2022.100670.

15. Chadi, K., Bencid, A., "Design effect of a mini-channel heat sink using additive manufacturing". Sustainable Polymer & Energy 3, 10004, 2025.https://doi.org/10.70322/spe.2025.10004

16. Moraveji, M. K., Ardehali, R. M., Ijam, A., "CFD investigation of nanofluid effects (cooling performance and pressure drop) in mini-channel heat sink.", International Communications in Heat and Mass Transfer. Vol. 40, pp.58-66, 2013.https://doi.org/10.1016/j.icheatmasstransfer.2012.10.021

17. Ghadhban, F. N., Jaffal, H. M., " Numerical investigation on heat transfer and fluid flow in a multi-minichannel heat sink: Effect of channel configurations," Results in Engineering, Vol. 17,100839,2023.https://doi.org/10.1016/j.rineng.2022.100839.

18. Al-Neama, A. F., Khatir, Z., Kapur, N., Summers, J., Thompson, H. M., "An experimental and numerical investigation of chevron fin structures in serpentine mini-channel heat sinks", Int. J. Heat Mass Transf. 120, 1213-1228, 2018.https://doi.org/10.1016/j.ijheatmasstransfer.2017.12.092